Kambham and Ramarakula
Satellite Navigation (2022) 3:21
https://doi.org/10.1186/s43020-022-00082-2

Satellite Navigation
https://satellite-navigation.springeropen.com/

ORIGINAL ARTICLE Open Access

An efficient approach for anti-jamming in IRNSS receivers using improved PSO based parametric wavelet packet thresholding

Jacob Silva Lorraine Kambham* and Madhu Ramarakula

Abstract

The Indian Regional Navigation Satellite System provides accurate positioning service to the users within and around India, extending up to 1500 km. However, when a receiver encounters a Continuous Wave Interference, its positioning accuracy degrades, or sometimes it even fails to work. Wavelet Packet Transform (WPT) is the most widely used technique for anti-jamming in Global Navigation Satellite System receivers. But the conventional method suffers from threshold drifting and employs inflexible thresholding functions. So, to address these issues, an efficient approach using Improved Particle Swarm Optimization based Parametric Wavelet Packet Thresholding (IPSO-PWPT) is proposed. Firstly, a new parameter adaptive thresholding function is constructed. Then, a new form of inertia weight is presented to enhance the performance of PSO. Later, IPSO is used to optimize the key parameters of WPT. Finally, the implementation of the IPSO-PWPT anti-jamming algorithm is discussed. The performance of the proposed technique is evaluated for various performance metrics in four jamming environments. The evaluation results manifest the proposed method's efficacy compared to the conventional WPT in terms of anti-jamming capability. Also, the results show the ability of the new thresholding function to process various signals effectively. Furthermore, the findings reveal that the improved PSO outperforms the variants of PSO.

Keywords: Continuous wave interference (CWI), IRNSS, Particle swarm optimization (PSO), Wavelet packet transform (WPT)

Introduction

Global Navigation Satellite System (GNSS) provide the users with position, velocity, and timing services anytime and anywhere. The utilization of GNSS in diverse applications is growing rapidly due to the increasing demand for location-based services. At present, the United States' Global Positioning System (GPS), Russia's GlObal NAvigation Satellite System (GLONASS), European Galileo, and China's BeiDou Navigation Satellite System (BDS) are the fully operational GNSS. In contrast, Indian Regional Navigational Satellite System (IRNSS) and Japan's Quasi-Zenith Satellite System (QZSS) are independent and autonomous regional navigation systems. As GNSS uses spread spectrum technology, it possesses inherent anti-jamming capability. However, as the GNSS satellites are placed at an altitude of nearly 20,000 km to more than 30,000 km, the signal's strength will be very weak when it reaches a receiver. Hence, the GNSS signals are easily prone to intentional (jamming) and unintentional interferences.

IRNSS, developed by the Indian Space Research Organization (ISRO), is a regional navigation satellite system. It utilizes the L5 band (1176.45MHz) and S-band (2492.028 MHz) frequencies for navigation solutions. However, the S-band of IRNSS is usually congested by the signals from various unintentional sources such as Wireless Fidelity (Wi-Fi), Bluetooth, and Industrial Scientific Medical (ISM) band (Jagiwala & Shah, 2019).

*Correspondence: jacobsilvalorraine@yahoo.com

Department of ECE, University College of Engineering, JNTUK, Kakinada, Andhra Pradesh 533003, India

Unintentional interference to the L5 band includes the pulsed signals from Tactical Air Navigation (TACAN), Distance Measuring Equipment (DME), Joint Tactical Information Distribution System (JTIDS), and Multifunctional Information Distribution System (MIDS) (Pena et al., 2020). In contrast, civilian jammers like Personal Privacy Devices (PPD) act as intentional ones. These sources of interference will degrade the accuracy of the IRNSS system or disrupt the operation completely. Therefore, to enhance the performance, effective countermeasures must be developed.

The literature reports several detection and mitigation techniques for the suppression of interference in GNSS receivers (Borio, 2021; Fadaei, 2016; Morales-ferre et al., 2019; Silva Lorraine & Ramarakula, 2021a). In addition, many works were done to deal with the interference of IRNSS signals (Dey et al., 2019, 2021; Jagiwala & Shah, 2019, 2021; Lineswala & Shah, 2019; Lineswala et al., 2019; Silva Lorraine & Ramarakula, 2021b, 2021c). Recently, a new framework for detecting GNSS jamming in moving platforms with a low computational burden was proposed (Sharifi-tehrani et al., 2020). On the other hand, jamming mitigation techniques are commonly categorized into spatial domain (Li et al., 2011; Jiaqi Zhang et al., 2019), frequency domain (Borio et al., 2008; Capozza et al., 2000; Varshney & Jain, 2013), time-domain (Anyaegbu et al., 2008; Mao, 2008), and Time-Frequency (TF) domain methods (Musumeci & Dovis, 2013; Ouyang & Amin, 2001; Wang et al., 2019). Spatial domain methods that use antenna arrays effectively mitigate narrowband and wideband interferences. However, they suffer from high cost, additional hardware required in the GNSS receiver, and computational complexity. In adaptive filtering-based methods, the jamming is estimated in frequency or time domain. These methods are suitable for the mitigation of narrowband jamming in low-power and low-cost applications. However, they require the prior knowledge about the jamming signal to have an acceptable anti-jamming performance. Also, single domain techniques like time or frequency domain are less effective in recovering the navigation signal, as the signal will be buried mostly in noise and interference when a receiver is operating in a severe interference environment. This could be resolved by TF domain techniques as the interfered signal could be represented in both domains. Wavelet Transform (WT) is the most prominent TF domain technique that has gained much attention in various applications like image processing (Nisha & Mohideen, 2016), signal processing (El-Dahshan, 2011; X. Zhang et al., 2017), multipath mitigation in GPS receivers (Satirapod & Rizos, 2005), as well as to mitigate various types of interference in GNSS receivers (Chien, 2018; Chien et al., 2017; Mosavi et al., 2015; Musumeci & Dovis, 2013; Silva Lorraine & Ramarakula, 2021b, 2021c).

WT is a well-known time scale transform. The signal received by WT is analyzed at various scales, and then its characteristics are extracted in both the time and frequency domains simultaneously. As a result, it works well against various types of jammers. Wavelet Packet Transform (WPT) is a generalization of the WT. It decomposes both the low-frequency and high-frequency components, thereby providing a uniform frequency band division. Hence, WPT is preferable to WT and it is the widely used technique as the information about both frequency components is vital in anti-jamming applications. However, the performance of wavelet-based methods is determined by the level of decomposition, wavelet function, threshold selection rule, and the thresholding function chosen. Among these parameters, the threshold selection rule and thresholding function are the most significant ones, which determine how well the interference can be suppressed while preserving the desired signal. The literature shows that the threshold obtained by the universal thresholding method drifts under different jamming scenarios (Chien, 2018). Furthermore, a higher threshold can compromise the desired components, while a lower threshold can retain the undesired components. Hence, estimating a reliable threshold under all the jamming scenarios is needed as threshold estimation significantly influences the anti-jamming effects of GNSS signals. Also, the works in the literature (Chien, 2018; Mosavi et al., 2015; Pashaian et al., 2016) use the traditional non-parametric thresholding functions (like soft and hard), which shrink the signal coefficients based on a fixed structure and reduce the flexibility to process various contaminated signals. So, this has motivated the authors to propose an efficient approach to improve the adaptive performance of WPT for anti-jamming. Given the above concerns, the following are the main contributions of this paper

(a) To overcome the limitations of the traditional thresholding functions, a new parameter adaptive thresholding function is designed to induce the flexibility in processing various signals.
(b) To determine an optimum threshold that can modify the wavelet coefficients in a way that results in noise and interference cancellation, an Improved Particle Swarm Optimization (IPSO) algorithm is proposed.
(c) To enhance the performance of conventional PSO by providing a better trade-off between exploration and exploitation, a new inertia weight adjustment strategy is introduced in the proposed IPSO algorithm.

To the best of the author's knowledge, the implementation of IPSO-based WPT with a parameter adaptive thresholding function to mitigate jamming in IRNSS receivers has not been done. The remaining sections are arranged in the following order. In "Signal modeling" section , modeling of the received and jamming signals is discussed. "Theoretical background" section focuses on the basic concept of WPT. Section "Proposed anti-jamming methodology" introduces the construction of the adaptive thresholding function, the adjustment strategy of inertia weight to modify standard PSO, the proposed anti-jamming scheme, and the computational complexity of the proposed algorithm. The findings are presented and discussed in "Results and discussions" section, and the conclusions are summarized in "Conclusion" section.

Signal modeling

Received signal model

The signal acquired at the receiver's front end can be modeled as

$$r(t) = s(t) + i(t) + n(t) \tag{1}$$

where $r(t)$, $i(t)$, and $n(t)$ represent the received signal, jamming signal, and the Additive White Gaussian Noise (AWGN) with variance σ^2, respectively, and $s(t)$ is the broadcasted navigation signal, written as

$$s(t) = \sqrt{2P_0}[D(t) \oplus C(t)]\cos(2\pi f_0 t + \theta) \tag{2}$$

where P_0 denotes the GNSS signal power, $D(t)$ represents the navigation data (± 1), and $C(t)$ is the Pseudo-Random Noise (PRN) sequence. For IRNSS, the PRN codes for Standard Positioning Service (SPS) are similar to GPS Code Acquisition (C/A) codes, with a chip rate of 1.023 MHz, f_0, and θ represent the carrier center frequency and phase delay, respectively.

The signal is then processed by a bandpass filter, amplifier, and mixer. The mixer down-converts the signal to an Intermediate Frequency (IF). Later, the analog IF signal is converted into digital by the Analog to Digital Converter (ADC) at a sampling rate $f_s = 1/T_s$, where T_s is the sampling time. The digital IF signal can be represented as

$$r[k] = s[k] + i[k] + n[k] \tag{3}$$

where $r[k]$, $s[k]$, $i[k]$, and $n[k]$ represent the digital versions of $r(t)$, $s(t)$, $i(t)$, and $n(t)$ respectively. k is the discrete-time index.

The output of the ADC is then passed through the jamming suppression unit, acquisition, tracking, and navigation units to process the signal further. Figure 1 shows the system architecture of an anti-jamming GNSS receiver. Jammer canceller uses signal processing techniques, like the proposed IPSO-based parametric WPT technique, and predicts the jamming signal $\tilde{i}[k]$. Thereafter, the jamming signal is subtracted from the received signal to obtain the interference-free GNSS signal $\tilde{s}[k]$.

Jamming signal model

To observe the robustness of the proposed anti-jamming algorithm, both stationary and non-stationary Continuous Wave Interferences (CWI), which are commonly used against the GNSS receivers, have been considered. They are single-tone CWI (SCWI), multi-tone CWI (MCWI), and chirp CWI (CCWI).

SCWI is one of the most impactful stationary interferences because of its easy design and implementation. Its spectral bandwidth tends to zero. Hence, in the case of a constant jamming power, most of the power of SCWI will be centralized at a single frequency. Therefore, it affects the GNSS signal to the most extent.

MCWI is a type of interference in which more than one interferer disrupts the GNSS signal. As most of the existing techniques work less effectively in the case of a multi-tone jammer, MCWI has been considered.

The non-stationary interference is usually characterized by linear CCWI. The frequency of the chirp signal increases (up-chirp) or decreases (down-chirp) with time. However, if the chirp frequency varies rapidly, sometimes, it can even make the jamming mitigation methods fail (Gao et al., 2016). Hence, CCWI with two different sweep bandwidths has been considered to observe the effectiveness of the proposed technique against various frequency sweeps.

The jamming signals can be modeled as follows

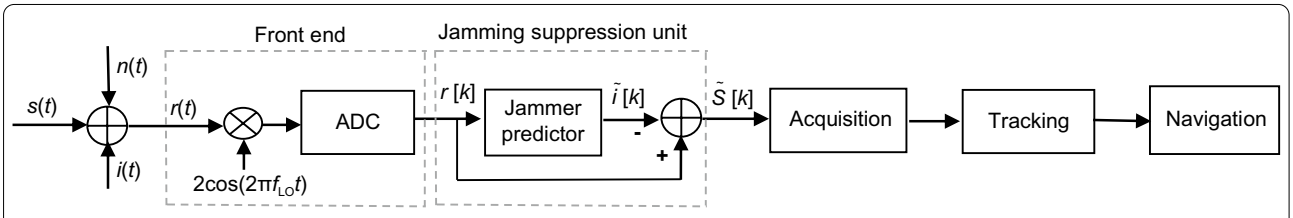

Fig. 1 Block diagram of anti-jamming GNSS receiver

(a) SCWI

$$i_{scwi}[k] = \sqrt{2P_i}\cos\left(2\pi f_i k + \theta_i\right) \quad (4)$$

where P_i represents the power of SCWI, f_i denotes the jamming signal frequency, and θ_i is the jamming signal's phase.

(b) MCWI

$$i_{mcwi}[k] = \sum_{n=1}^{N} \sqrt{2P_{i_n}}\cos\left(2\pi f_{i_n} k + \theta_{i_n}\right) \quad (5)$$

where P_{i_n},f_{i_n}, and θ_{i_n} represents the power, frequency, and phase of the nth jammer, respectively, and N denotes the number of jammers.

(c) CCWI

$$i_{chirp}[k] = \sqrt{2P_i}\cos\left[2\pi\left(f_i \pm \frac{c}{2}k\right)k + \theta_i\right] \quad (6)$$

where P_i represents the chirp jammer's power, f_i indicates the starting frequency (at time t = 0), θ_i is the chirp signal's phase, and c denotes the chip rate. '+' is considered for an up-chirp, while '–' is considered for a down-chirp.

Theoretical background

Transform Domain (TD) techniques are advanced signal processing techniques that represent the received signal in a different domain. Therefore, they can easily identify, isolate, process, and remove the interference in a better way while preserving the desired signal. TD techniques are usually implemented after the ADC stage in a GNSS receiver. A well-known transformation is a time-frequency representation in which the signal can be represented over time and frequency simultaneously.

Some of the most used time–frequency anti-jamming methods in GNSS receivers are Short-Time Fourier Transform (STFT) (Abedi et al., 2018; Ouyang & Amin, 2001), Matched Signal Transform (MST) (Shen & Papandreou-suppappola, 2005), Wigner Ville Distribution (WVD) (Fadaei, 2016), and WT (Chien, 2018; Mosavi et al., 2015, 2017; Musumeci & Dovis, 2013). In recent years, wavelet-based methods have also been used to mitigate CW jamming (Jagiwala & Shah, 2021; Silva Lorraine & Ramarakula, 2021b, 2021c) and out-of-band Wi-Fi interference on IRNSS S-band signals (Jagiwala & Shah, 2019). STFT is a windowed-Fourier transform that uses a fixed window; hence, the time–frequency resolution of STFT remains constant. Therefore, it is not suitable for non-stationary signals. MST works well only when the interference characteristics are known a priori. Moreover, the computational complexity of MST is higher than STFT. The WVD has a good time–frequency resolution, but suffers from cross-term interference in the case of multi-component signals. So, to reduce the cross-term interference, pseudo-WVD has been introduced; however, it suffers from energy leakage at the beginning and end of the TF plane (Lv & Qin, 2019). In wavelet transform, a scalable window is used, i.e., a wider window for low-frequency analysis and a narrower window for high-frequency analysis. Hence, WT is an excellent tool to deal with different kinds of interference as it provides a good trade-off between time and frequency resolution. WT is a linear, square-integrable transform that has a kernel (mother transform). All the other wavelets $\psi_{s,\tau}(t)$ can be obtained by shifting and scaling (compressing and expanding) the mother wavelet as

$$\psi_{s,\tau}(t) = \frac{1}{\sqrt{s}}\psi\left(\frac{t-\tau}{s}\right) \quad (7)$$

where $\psi(t)$ represents the mother wavelet, s is the scaling parameter, and τ is the shifting parameter.

Continuous Wavelet Transform (CWT) is computed by continuously shifting the scaled analyzing function over a signal for each scale. As a result, it suffers from redundancy issues and is therefore unsuitable for practical applications. So, to overcome this, Discrete Wavelet Transform (DWT), which uses discrete scales and translations, has been introduced. Discrete wavelets are obtained by shifting and scaling the mother wavelet as

$$\psi_{i,j}(t) = \frac{1}{\sqrt{s_0^i}}\psi\left(\frac{t - j\tau_0 s_0^i}{s_0^i}\right) \quad (8)$$

where s_o is the dilation or scaling parameter, τ_o is the translation or shifting parameter that depends on the dilation parameter, i and j are both integers, and $\frac{1}{\sqrt{s_0^i}}$ normalizes the energy across various scales.

DWT is implemented using a recursive filter scheme. First, the signal is sent through a High Pass Filter (HPF) and Low Pass Filter (LPF). The output of the HPF is known as the detail coefficient, while the output of the LPF is known as the approximation coefficient. The approximation coefficient is then further decomposed iteratively, whereas the detail coefficient is retained. Therefore, due to the non-uniform spectral decomposition, frequency localization at higher frequency levels is lost for time localization.

Wavelet packets were first introduced by Coifman and Meyer (Kaiser, 1994). In WPT, both the approximation and detail components are further decomposed at each level. Hence, the reconstruction of the signal

is obtained by summing the approximation parts and detail parts as shown below

$$\tilde{r}[k] = \sum_{l=1}^{L} a_l[k] + \sum_{l=1}^{L} d_l[k] \tag{9}$$

where $\tilde{r}[k]$ indicates the reconstructed signal, L represents decomposition depth,$a_l[k]$ and $d_l[k]$ are the approximation and detail components at the level l.

WPT offers uniform spectral coverage, better frequency resolution, and signal analysis. As the signal details of both the low and high-frequency components are desirable for interference suppression, WPT, which has a higher frequency resolution than DWT, is considered in this work. Fig. 2 shows the decomposition and reconstruction of the received signal using WPT at decomposition level 2. HP and LP stand for high pass and low pass. While $g[k]$, $h[k]$ symbolize LP and HP filters at the decomposition side, $g^1[k]$, $h^1[k]$ are LP and HP filters at the reconstruction side.

Proposed anti-jamming methodology

Construction of parametric wavelet thresholding function

The thresholding function defines the various estimation approaches for the wavelet coefficients. The main idea behind the thresholding function is to remove the smaller wavelet coefficients and retain the larger ones. The two most prominent thresholding functions are hard and soft thresholding. However, hard thresholding gets limited because of the discontinuity at the threshold value ($\pm T$). As a result, it causes fluctuation while reconstructing the signal. On the other hand, soft thresholding is better in continuity, but it gets limited by the deviation between the estimated and actual wavelet coefficients during the reconstruction (He et al., 2015). Therefore, to obtain a trade-off between the two thresholding functions, a new parameter adaptive wavelet thresholding function based on the Softsign function has been constructed to have a better anti-jamming effect. The graph of the Softsign function looks very similar to the hyperbolic tangent function (tanh). However, the Softsign converges in a polynomial form, while the tanh function converges exponentially. Soft sign is expressed as

$$f(x) = \frac{x}{1 + |x|} \tag{10}$$

The properties of Softsign are defined as follows.

1. The range of the function is $(-1, 1)$, and its domain is $(-\infty, +\infty)$.
2. It obeys monotonicity.
3. It possesses two horizontal asymptotes at $f(x) = 1$ and $f(x) = -1$.
4. It is differentiable in its domain.

Based on Eq. (10), the expression for the new Softsign Thresholding Function (SSTF) is constructed as

$$\tilde{C} = f(C) = \begin{cases} \operatorname{sgn}(C)(|C| - T) + T\left(\frac{(C-T)\beta/T}{1+|(C-T)\beta/T|}\right), & C > T \\ 0, & |C| \le T \\ \operatorname{sgn}(C)(|C| - T) + T\left(\frac{(C+T)\beta/T}{1+|(C+T)\beta/T|}\right), & C < -T \end{cases} \tag{11}$$

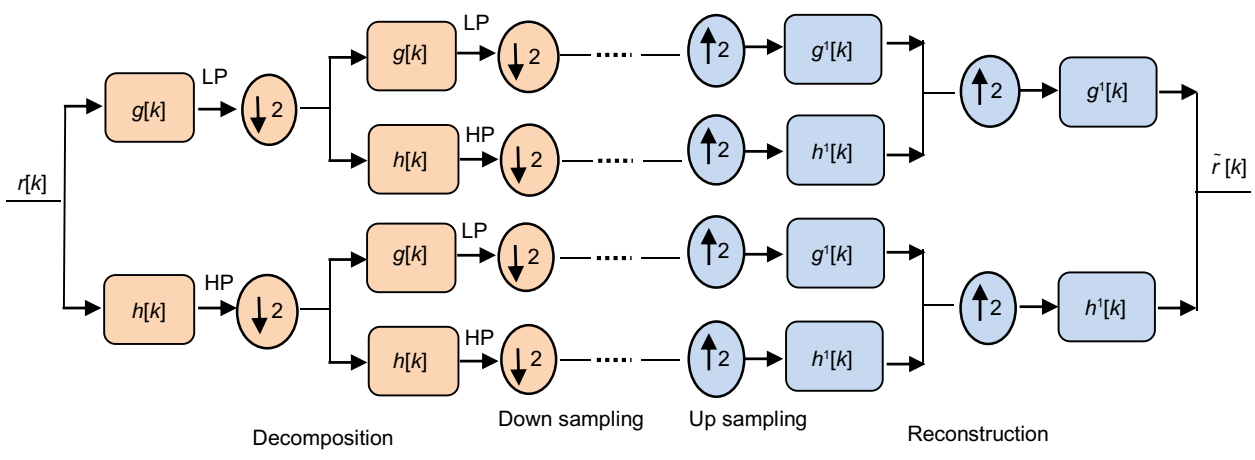

Fig. 2 Signal decomposition and reconstruction structure by WPT

where $\tilde{C}$ is the thresholded coefficient, C is the wavelet coefficient on a particular band, and *sgn* represents the signum function whose value is 1 for $C>0$, 0 for $C=0$, and -1 for $C<0$. T is the threshold, and β is the shape tuning parameter that characterizes the function $f(C)$. The value of β lies in the range of $(0,+\infty)$. The shape parameter offers more adjustability to the function. When β approaches 0, this new function acts as a soft thresholding function; when β approaches ∞, it acts as a hard thresholding function.

The properties and proof of the new thresholding function are presented below.

Theorem 1 *The SSTF function is continuous in its domain* $(-\infty,+\infty)$.

Proof

From the definition of continuity, the new function should be continuous in the ranges of $(-\infty,-T)$,$(-T,+T)$ *and* $(+T,+\infty)$. *Therefore, the continuity of SSTF at* $-T$ *and* $+T$ *points can be proved as follows.*

When $C > T$ the SSTF function can be rewritten as

$$f(C) = C - T + T\left(\frac{(C-T)\beta/T}{1+(C-T)\beta/T}\right) \tag{12}$$

So,

$$\lim_{C\to T^+} f(C) = \lim_{C\to T^+}\left(C - T + T\left(\frac{(C-T)\beta/T}{1+(C-T)\beta/T}\right)\right)$$

$$= (T-T) + T\left(\frac{0}{1+0}\right) \tag{13}$$

$$= 0$$

$$\text{when } |C| \le T \text{ , we get } f(C) = 0 \tag{14}$$

$$\text{Therefore, } \lim_{C\to T^-} f(C) = 0 \text{ and } f(T) = 0 \tag{15}$$

So, from Eq. (13) and Eq. (15), we obtain that $\lim_{C\to T^-} f(C) = \lim_{C\to T^+} f(C) = f(T)$.

Hence at $C=T$, the function is continuous. Likewise, at $C=$-T, the function's continuity can be verified. As a result, $f(C)$ is defined as a continuous function in the domain $(-\infty,+\infty)$.

Comment: It can be observed that the limitation of the hard thresholding function, i.e., discontinuity at the threshold $\pm T$, can be overcome by the SSTF function.

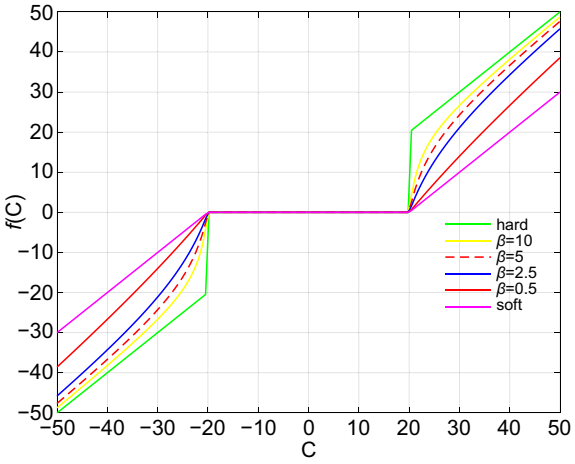

Fig. 3 Comparison of thresholding functions: Hard, Soft and SSTF

Theorem 2 *The asymptote of the SSTF function is* $f(C) = C$.

Proof

As per the definition, $y = L$ *is a horizontal asymptote of the function* $y = f(x)$ *if* $\lim_{x\to+\infty} f(x) = L$ *or* $\lim_{x\to-\infty} f(x) = L$

Therefore, when $C \to +\infty$

$$\lim_{C\to+\infty}\frac{f(C)}{C} = \lim_{C\to+\infty}\frac{C - T + T\left(\frac{(C-T)\beta/T}{1+(C-T)\beta/T}\right)}{C} \tag{16}$$

$$\lim_{C\to+\infty}\frac{f(C)}{C} = \lim_{C\to+\infty}\left[1 - \frac{T}{C} + \frac{T}{C}\left(\frac{(C-T)\beta/T}{1+(C-T)\beta/T}\right)\right] = 1$$

Similarly, when $C \to -\infty$

$$\lim_{C\to-\infty}\frac{f(C)}{C} = \lim_{C\to-\infty}\frac{C - T + T\left(\frac{(C-T)\beta/T}{1+(C-T)\beta/T}\right)}{C} = 1 \tag{17}$$

So that

$$\lim_{C\to+\infty}(f(C) - C) = \lim_{C\to+\infty}\left(-T + T\left(\frac{(C-T)\beta/T}{1+(C-T)\beta/T}\right)\right) = 0 \tag{18}$$

Hence, $f(C) = C$ is an asymptote of SSTF. Similarly, it can be proved for the other case as well.

Comment: From theorem 2, it can be observed that as C increases, $f(C)$ gradually approaches C. Hence, it overcomes the limitation of the soft thresholding function

as it reduces the difference between the actual and estimated coefficients.

Theorem 3 *SSTF is a higher-order differentiable function in the domain* $(-\infty, -T]$ *and* $[+T, +\infty)$.

Proof

Any function obtained by the mathematical operations of the elementary functions is an elementary function. So, as per the elementary function property, SSTF is a high-order differentiable function.

Comment: As SSTF satisfies theorem 3, it helps to reconstruct the signal smoothly.

Figure 3 shows the comparative analysis of hard, soft, and SSTF thresholding functions at a threshold value of 20. To observe the behavior of SSTF, the adjustable parameter β is varied. It can be perceived from Fig. 3 that the new function offers a trade-off strategy between the two traditional thresholding functions.

Improved particle swarm optimization (IPSO)

The determination of the threshold plays a major role in jamming signal estimation. If the threshold value is very small, it can retain the undesired components, and if the threshold is very large, it can filter out the desired components. The universal threshold rule is the most used one among all the threshold rules. However, it suffers from threshold drifting (Chien, 2018). Similarly, the choice of the new thresholding function's shape tuning parameter affects the reconstruction of the signal. Generally, the tuning parameter is selected iteratively. But as it adjusts the thresholding function, it is of utmost importance to find the shape tuning parameter. So, to address these issues, optimization algorithms have been employed. PSO has been chosen due to its simplicity, easy implementation, high accuracy, faster convergence, lesser control parameters, and computational efficiency (Zang et al., 2021; Zhang et al., 2014). Hence, owing to its numerous advantages, PSO has gained a lot of attention in many areas like signal denoising (Zhang et al., 2017), load forecasting (Kumar & Veerakumari, 2012), filter design (Sharma et al., 2016), image processing (Satish & Kumar, 2020), fault diagnosis (Zhang & Wang, 2020), etc. However, PSO suffers from the local optimum problem. Therefore, the strategy of adaptive inertia weight has been implemented to enhance the efficacy of conventional PSO.

Standard PSO algorithm

PSO is the most extensively used swarm intelligence technique developed by Kennedy and Eberhart in 1995 (Kennedy and Eberhart, 1995). The swarm behavior of birds flocking has been the inspiration for PSO. The bird is considered as a particle in PSO. Through its efforts and with the cooperation of the neighboring particles, the particle will search for its optimal solution. The process of the PSO is described as follows. First, the population size, velocity, position, and the number of iterations are initialized. The particles move through the dimensional solution space with randomly assigned velocities. Each particle's performance is evaluated using a fitness function. Then, as per the local best (*Lbest*) and global best (*Gbest*) fitness values, the particle's velocity and position are updated as

$$V_{pd}^{j+1} = w^j V_{pd}^j + c_1 r_1 (Lbest_{pd}^j - X_{pd}^j) + c_2 r_2 (Gbest_d^j - X_{pd}^j) \tag{19}$$

$$X_{pd}^{j+1} = X_{pd}^j + V_{pd}^{j+1} \tag{20}$$

where the pth particle's velocity and position factor in the dth dimension is indicated by V_{pd} and X_{pd} , the current iteration number is denoted by j, *Lbest* represents the particle's best position, and *Gbest* is the swarm's best position. c_1 is the cognitive acceleration factor that pushes the particles towards *Lbest*, c_2 is the social acceleration factor that pushes the particle towards *Gbest*, r_1, r_2 denotes the random numbers between 0 and 1, and w represents the inertia weight.

The PSO process is iterated until it reaches the maximum number of iterations or the termination criteria are met.

Modified inertia weight formulation

The inertia weight is an important parameter of PSO that governs the effect of the previous particle's velocity on the current particle's velocity. A larger inertia weight produces a better global search, whereas a smaller inertia weight produces a better local search. A good global search prevents the particle from being stuck at the local optimum easily, and a good local search ensures faster convergence speed and better accuracy. So, to provide a better trade-off between exploration (global search) and exploitation (local search), inertia weight (w) must be chosen properly. In 1998, Shi and Eberhart (1998) first introduced a constant inertia weight into the original PSO to provide a balance between the global and local search. Many adaptive inertia weight strategies were

later reported in the literature for enhancing PSO performance. Some classical strategies include random inertia weight (Eberhart & Shi, 2001), linear time-varying inertia weight (Shi & Eberhart, 1999), and non-linear time-varying inertia weight (Chatterjee & Siarry, 2006). In a random inertia weight, w changes randomly and can be adapted to dynamic systems (Eberhart & Shi, 2001).

Whereas in the time-varying inertia weight strategy, w varies linearly or non-linearly with time in a decreasing or increasing manner. These strategies are useful in most applications for improving the performance of PSO. However, to have a better PSO performance, it was ascertained that inertia weight should be higher initially and decreased later (Shi & Eberhart, 1998). This facilitates a finer global exploration at the initial stages and local exploration at the latter stages. But, linearly decreasing inertia weight strategies were found to be ineffective for dynamic systems (Eberhart & Shi, 2001). So, non-linear decreasing inertia weight strategies have gained much attraction. Therefore, a new non-linear decreasing inertia weight strategy based on the Softsign function is developed in this work. As the Softsign function is simple and easy to implement, the Softsign Inertia Weight (SSIW) is considered in this paper and formulated as

$$w = w_{\min} + (w_{\max} - w_{\min}) \frac{\left[\left(iter_{\max} - j\right)/iter_{\max}\right]}{1 + \left[\left(iter_{\max} - j\right)/iter_{\max}\right]} \tag{21}$$

where w_{max} denotes the maximum value of inertia weight, w_{min} is the minimum value of inertia weight, j is the current iteration number, and $iter_{max}$ represents the maximum iteration number.

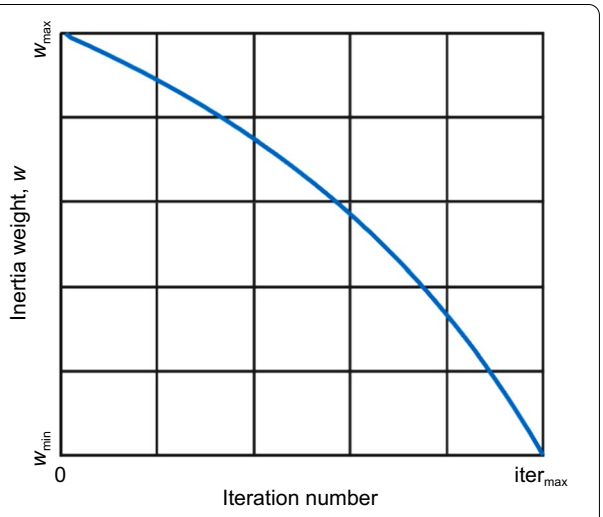

Fig. 4 Performance of SSIW

Figure 4 shows the variation of the proposed inertia weight with respect to the number of iterations. It can be observed that the SSIW strategy meets the demand of the global search at the initial stages and faster convergence at the latter stages.

Proposed improved PSO-based parametric WPT anti-jamming algorithm

Steps for the implementation of the proposed anti-jamming algorithm

Step 1: Wavelet packet decomposition

Initially, the wavelet function and decomposition level must be chosen. Then, WPT is used to decompose the received signal $r[k]$. The optimal tree structure of WPT is selected based on the Shannon entropy criterion.

The coefficients obtained after the decomposition process are represented as

$$C_l[k] = wp(r[k]) \tag{22}$$

where $C_l[k]$ is the wavelet coefficient on a particular band, and wp is the wavelet packet operator.

Step 2: Determine the optimal threshold (T) and shape tuning parameter (β) using IPSO.

1. Set the population size, maximum iteration number, search space dimension, particle velocity, and position. The problem's dimension is taken as the particle's position.
2. Fitness function formulation: The particle's fitness value is evaluated using the fitness function. In this work, the fitness function is formulated based on performance metrics. The following performance indices are considered.

Mean Square Error (MSE): MSE defines the accuracy of the anti-jamming algorithm. The lower the MSE value, the lesser the variation between the two signals is. If $s[k]$ is the original signal,$\tilde{s}[k]$ represents the reconstructed signal, k and M denote the sample number and signal length, then MSE is represented as

$$MSE = \frac{1}{M} \sum_{k=1}^{M} (\tilde{s}[k] - s[k])^2 \tag{23}$$

Mean Absolute Error (MAE): It is similar to MSE. The lower the value of MAE, the better the accu-

racy of the proposed technique is. It is represented as

$$MAE = \frac{1}{M}\sum_{k=1}^{M}\left|\tilde{s}[k] - s[k]\right| \tag{24}$$

Correlation Coefficient (CC): It measures the similarity between the reconstructed and original signals. The closer to 1 the value of CC is, the more similar the reconstructed signal and the original signal will be.

$$CC_{X,Y} = \frac{1}{M-1}\sum_{k=1}^{M}\left(\frac{x[k]-\bar{x}}{\sigma_x}\right)\left(\frac{y[k]-\bar{y}}{\sigma_y}\right) \tag{25}$$

where $x[k]$ and $y[k]$ are the two discrete sequences, $\bar{x}$ is the mean of x, $\bar{y}$ is the mean of y, and σ_x, σ_y denote the standard deviation of x and y, respectively.

Signal to Noise Ratio Improvement (SNR_{imp}): It measures the variation between the output and input SNR. The higher the value of SNR improvement is, the more accurate the anti-jamming algorithm will be. It is expressed as

$$SNR_{imp}(dB) = 10\log\frac{\sum_{k=1}^{M}(r[k]-s[k])^2}{\sum_{k=1}^{M}(\tilde{s}[k]-s[k])^2} \tag{26}$$

Accordingly, the MSE based fitness function is formulated as

$$\text{fitness} = \min(\text{MSE}) \tag{27}$$

A similar formulation has been adopted for MAE, while for CC and SNR_{imp}, PSO is used to find the maximum value.

3. Update the velocity and position using Eq. (19) and Eq. (20).

The inertia weight is calculated using the SSIW expressed in Eq. (21).

4. Update the swarm: The new position's fitness value is computed. If the present value is better than the previous *Lbest* then it is taken as *Lbest;* otherwise, the previous value is retained. Similarly, *Gbest* is updated accordingly.

5. Steps 3 and 4 are repeated until the maximum number of iterations is reached.

Step 3: Thresholding using SSTF

The resulting coefficients $C_l[k]$ are then thresholded using the new SSTF with the obtained optimal values (T, β) of the thresholding function as follows

$$\tilde{C}_l[k] = TF(C_l[k], T) \tag{28}$$

where $\tilde{C}$ represents the thresholded coefficient, T stands for the threshold, and TF denotes the thresholding operator.

Step 4: Signal reconstruction

Using inverse WPT, the signal is reconstructed from the thresholded coefficients as follows

$$\tilde{i}[k] = wp^{-1}(\tilde{C}_l[k]) \tag{29}$$

Due to its low signal strength, the navigation signal will be buried in noise and interference when it reaches

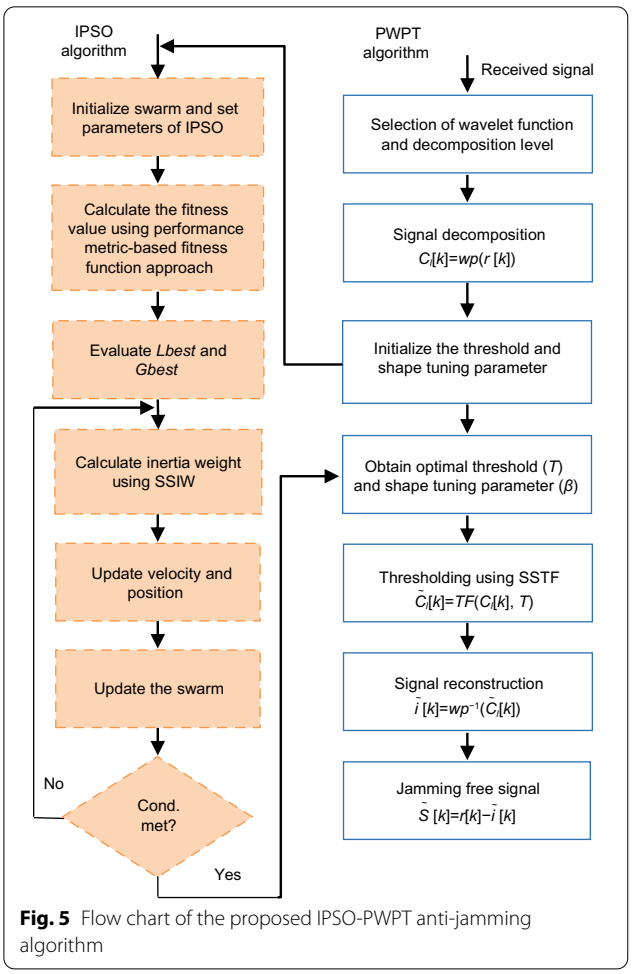

Fig. 5 Flow chart of the proposed IPSO-PWPT anti-jamming algorithm

the receiver. Therefore, the jamming signal is estimated from the WPT process. Later, the jamming signal is subtracted from the received signal to get the desired IRNSS signal $\tilde{s}[k]$.

The flowchart of the proposed anti-jamming approach is depicted in Fig. 5.

Computational complexity

The computational load of the proposed algorithm is induced mostly due to WPT (decomposition and reconstruction), thresholding operation, and IPSO.

The computational complexity of the wavelet packet analysis is specified by the decomposition level L, signal length M, and the wavelet filter length l_w. Signal reconstruction also takes the same number of filtering operations. Therefore, the total number of the operations performed for decomposition and reconstruction can be expressed as (Musumeci & Dovis, 2014):

$$O(L, M, l_w) = 2^{L+1} M(1 + l_w) \tag{30}$$

For the thresholding operation, assuming that the coefficients to be thresholded are n digit numbers, Eq. (11) gives a computational complexity of $O(n^2)$.

The computational cost of IPSO is obtained as follows. The computational cost of the original PSO algorithm is specified by initialization, evaluation, velocity, and position update (Song & Hua, 2020). Additionally, IPSO requires an inertia weight update. Therefore, their complexities are $O(Pd)$, $O(Pd)$, and $O(3Pd)$, where P and d represent the swarm size and the dimension of the solution space, respectively. Therefore, the total computational complexity of the IPSO algorithm is $O(Pd)$.

Results and discussions

To analyze the performance of the proposed IPSO-based Parametric Wavelet Packet Thresholding (IPSO-PWPT), four types of jamming signals with different levels of Jamming to Signal power Ratio (JSR) were taken into account. For SCWI, the jamming offset frequency was set close to the center frequency of the IRNSS signal to observe the jammer effect. MCWI was generated by combining four sinusoidal signals. For the generation of non-stationary signals, two types of CCWI were considered. In the first case, a linear CCWI with a sweep bandwidth of 10.72 MHz was taken, and the sweep period was set to 5000 samples long. In the second case, the sweep bandwidth was set to 10KHz with the same sweep period. For the generation of the IRNSS S-band signal, $D[k]$ was binomially distributed with values of ± 1, and PRN1 was used to generate $C[k]$. Table 1 presents the design parameters of IRNSS signal and jamming signals. The IPSO parameters considered for the simulation are furnished in Table 2. All the simulation experiments were carried out on the same computer, which had a 3.6GHz CPU frequency, 8GB of RAM, and MATLAB version of 2017b.

Table 1 Simulation parameters for IRNSS and jamming signals

Parameter description	Value
Signal (s)	IRNSS S-band
Processed signal bandwidth	2.046 MHz
Sampling frequency	56 MHz
Digital IF	16.221 MHz
SCWI offset frequency	0.5 MHz
MCWI offset frequency	0.2 MHz, 0.8 MHz, 1.3 MHz, 1.8 MHz
CCWI-1 sweep bandwidth	10.72 MHz
CCWI-2 Sweep bandwidth	10 kHz

Table 2 Simulation parameters of IPSO

Parameter	Description	Value
r_1, r_2	Random numbers	Uniformly distributed in the range of [0,1]
c_1, c_2	Acceleration coefficients	2
P	Population size	50
$iter_{\max}$	Maximum iteration number	100
d	Search dimension	2
W_{min}	Minimum inertia weight	0.4
W_{max}	Maximum inertia weight	0.9
T	Threshold value	[0,2]
β	Shape tuning parameter	[0,10]

Selection of threshold

Traditional threshold selection rules like the universal threshold (Mosavi et al., 2015), Rigrsure, Minimax, Sqtwolog, and other threshold selection methods mentioned in the literature for anti-jamming (Chien, 2018), (Pashaian et al., 2016) were considered to evaluate the performance of the optimization-based threshold approach.

Table 3 Summary of obtained threshold values

Threshold rule\type of jamming	Range of threshold values			
	SCW	MCW	CCW-1	CCW-2
Universal	6.37–7.81	6.15–7.79	5.88–6.99	5.49–6.91
Rigrsure	0.02–0.081	0.05–0.07	0.012–0.48	0.02–0.298
Minimax	2.8239	2.8239	2.8239	2.8239
Sqtwolog	4.2919	4.2919	4.2919	4.2919
Chien	0.01–0.075	0.049–0.065	0.011–0.449	0.024–0.276
Pashaian	7.95–9.74	7.67–9.72	7.34–8.72	5.70–7.17
SPSO based	1.85–2	1.7–2	1.86–2	1.84–2

The thresholding function was chosen as soft thresholding for all the threshold rule comparisons. Also, simulations were run for all the wavelet families when JSR varied from 30 to 60 dB, and Discrete Meyer (Dmey) wavelet was chosen based on the performance indices as it appears to perform well under all the jamming scenarios. The decomposition level was set to 4 as per the reference (Silva Lorraine & Ramarakula, 2021c). The four metrics mentioned in Eqs. (23) to (26) were selected as the comparative indices. The range of threshold values obtained by each method under JSR of 30 to 60 dB are listed in Table 3 for comparative purposes. Table 3 shows that the resulting value of universal, minimax, sqtwolog, and Pashaian threshold methods are very high, making the jammer parts to be compromised (Chien et al., 2017). Hence, the jamming signal cannot be estimated properly. Also, there seems to be threshold drifting for universal and Pashaian methods under various jamming scenarios. Minimax and sqtwolog are fixed form thresholds that do not depend on the signal characteristics but instead only on the signal length. As a result, the threshold is non-adaptive to the incoming signals. For rigrsure and Chien methods, the undesired components might be retained as the threshold is very low. Hence, they are ineffective in suppressing the jamming signal when only WPT technique is used. However, cascading WPT with

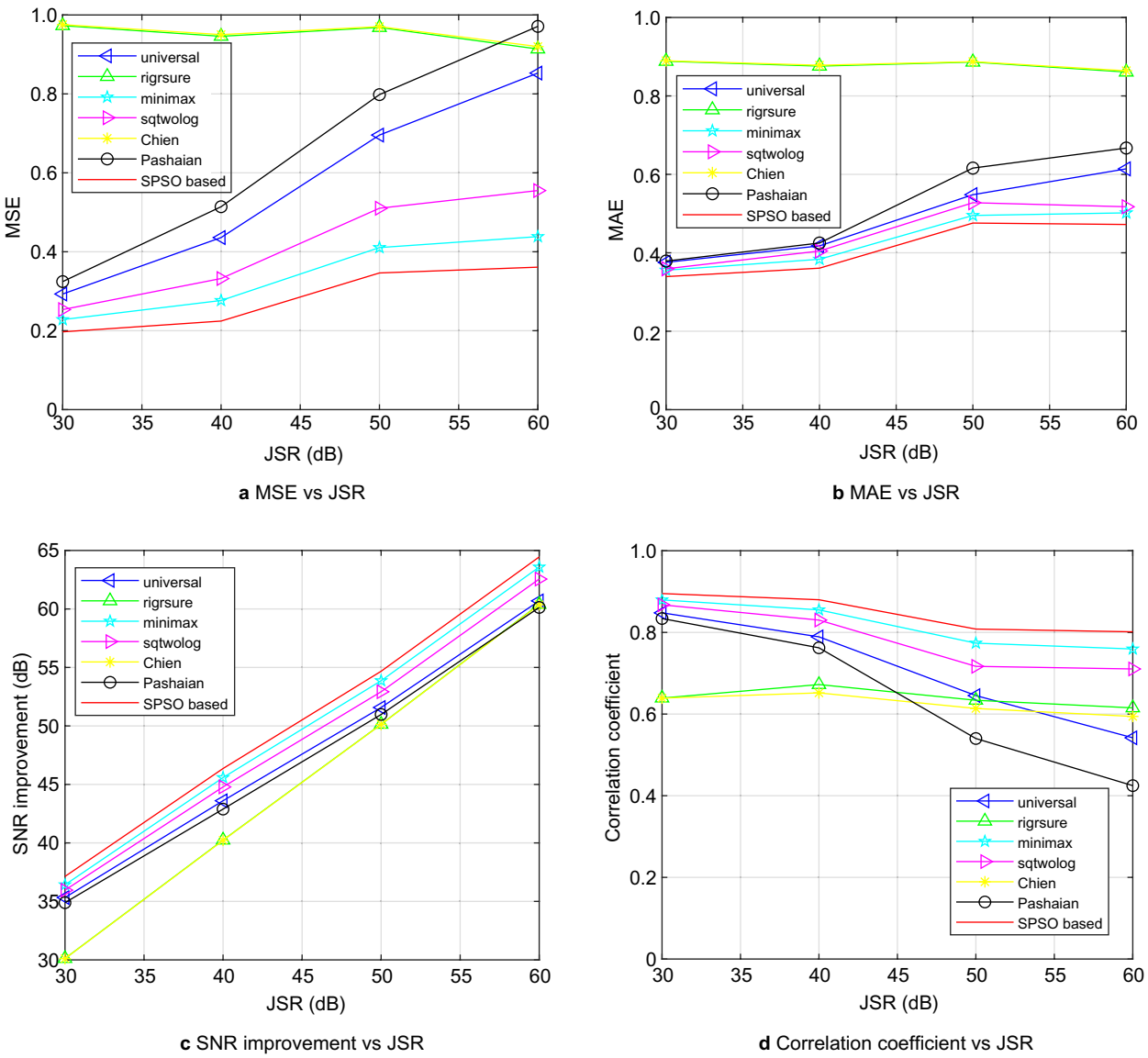

Fig. 6 Comparison of various thresholding rules under SCWI

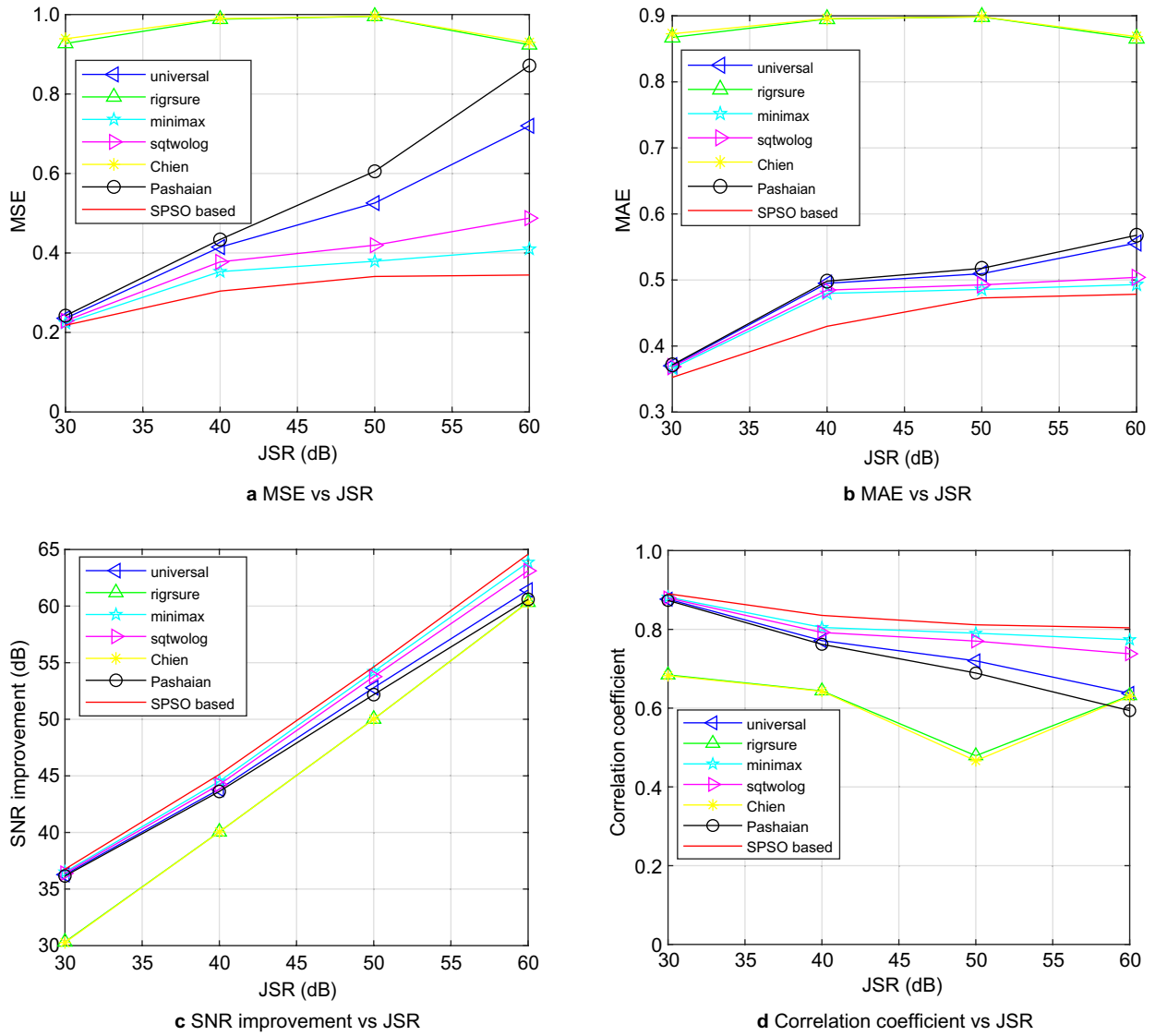

Fig. 7 Comparison of various thresholding rules under MCWI

other techniques might improve the performance (Chien, 2018). Therefore, in this paper, the feasibility of using optimization-based threshold selection is explored.

For the optimization-based threshold method, the threshold range was set to [0,2] as per the reference (Chien et al., 2017), and standard PSO (SPSO) was selected as an optimization technique for the comparison of threshold selection methods. Table 3 shows that the threshold values obtained by the proposed method provide a trade-off between high and low threshold values under all jamming scenarios. In addition, it addresses the issues of fixed threshold and threshold drifting. Figs. 6, 7, 8, 9 displays the performance of various threshold selection rules. It can be observed that the proposed optimization-based threshold (SPSO based) performs significantly better under SCWI, MCWI, CCWI case 1 (CCWI-1), and CCWI case 2 (CCWI-2) environments.

SCWI environment

Under the SCWI scenario, it is observed that the optimization-based threshold approach has an average improvement of 47% over universal, 70% over rigrsure, 16% over minimax, 30% over sqtwolog, 70% over Chein, and 54% over Pashaian threshold methods in terms of MSE. Similarly, an average improvement of 15%, 53%, 5%, 9%, 53%, and 19% in terms of MAE and 23%, 32%, 4%, 9%, 35%, and 40% in terms of CC over the respective threshold rule methods are noticed. In terms of SNR improvement,

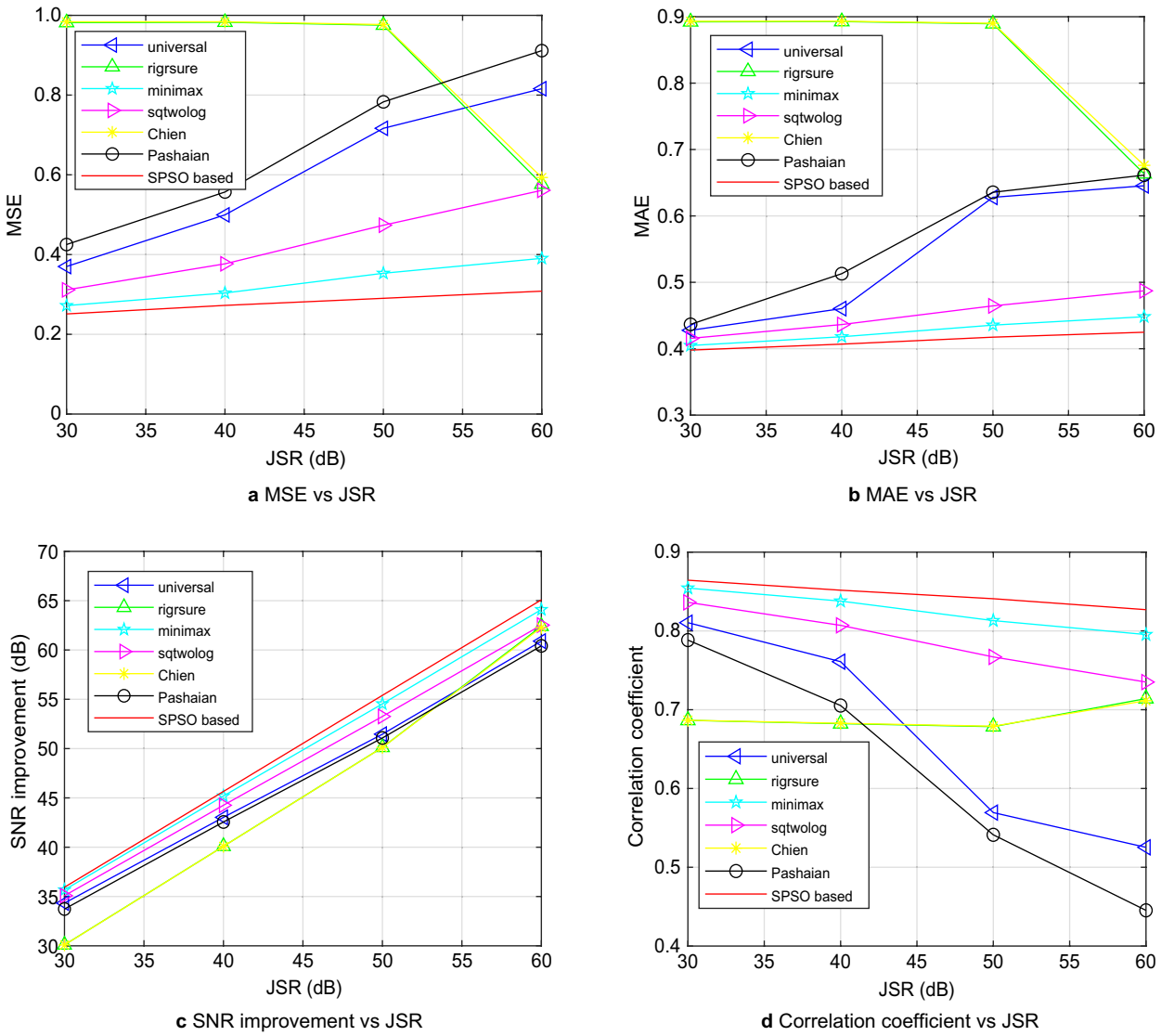

Fig. 8 Comparison of various thresholding rules under CCWI-1

a gain of 2.9 dB, 5.4 dB, 0.8 dB, 1.6 dB, 5.4 dB, and 3.4 dB over universal, rigrsure, minimax, sqtwolog, Chein, and Pashaian methods, respectively, is observed when the optimization-based threshold is used.

MCWI environment

Under multi-tone jamming environment, an average improvement of 30%, 69%, 11%, 18%, 69%, and 36% in terms of MSE, similarly, an average improvement of 10%, 51%, 5%, 6%, 51% and 11% in terms of MAE and 12%, 39%, 3%, 5%, 41% and 16% in terms of CC over universal, rigrsure, minimax, sqtwolog, Chein and Pashaian methods are noticed. In terms of SNR improvement, a gain of 1.7 dB, 5.1 dB, 0.5 dB, 0.9 dB, 5.1 dB, and 2.1 dB over the respective threshold rule methods is observed.

CCWI environment

An average improvement of 50%, 66%, 14%, 33%, 66%, and 55% under CCWI-1, and 45%, 68%, 17%, 31%, 69%, and 44% under CCWI-2 in terms of MSE is observed. Similarly, an average improvement of 22%, 50%, 3%, 8%, 50%, 25% under CCWI-1 and 10%, 52%, 5%, 8%, 52%, 14% under CCWI-2, in terms of MAE and 31%, 23%, 3%, 8%, 23%, 43% under CCWI-1 and 14%, 30%, 3%, 7%,

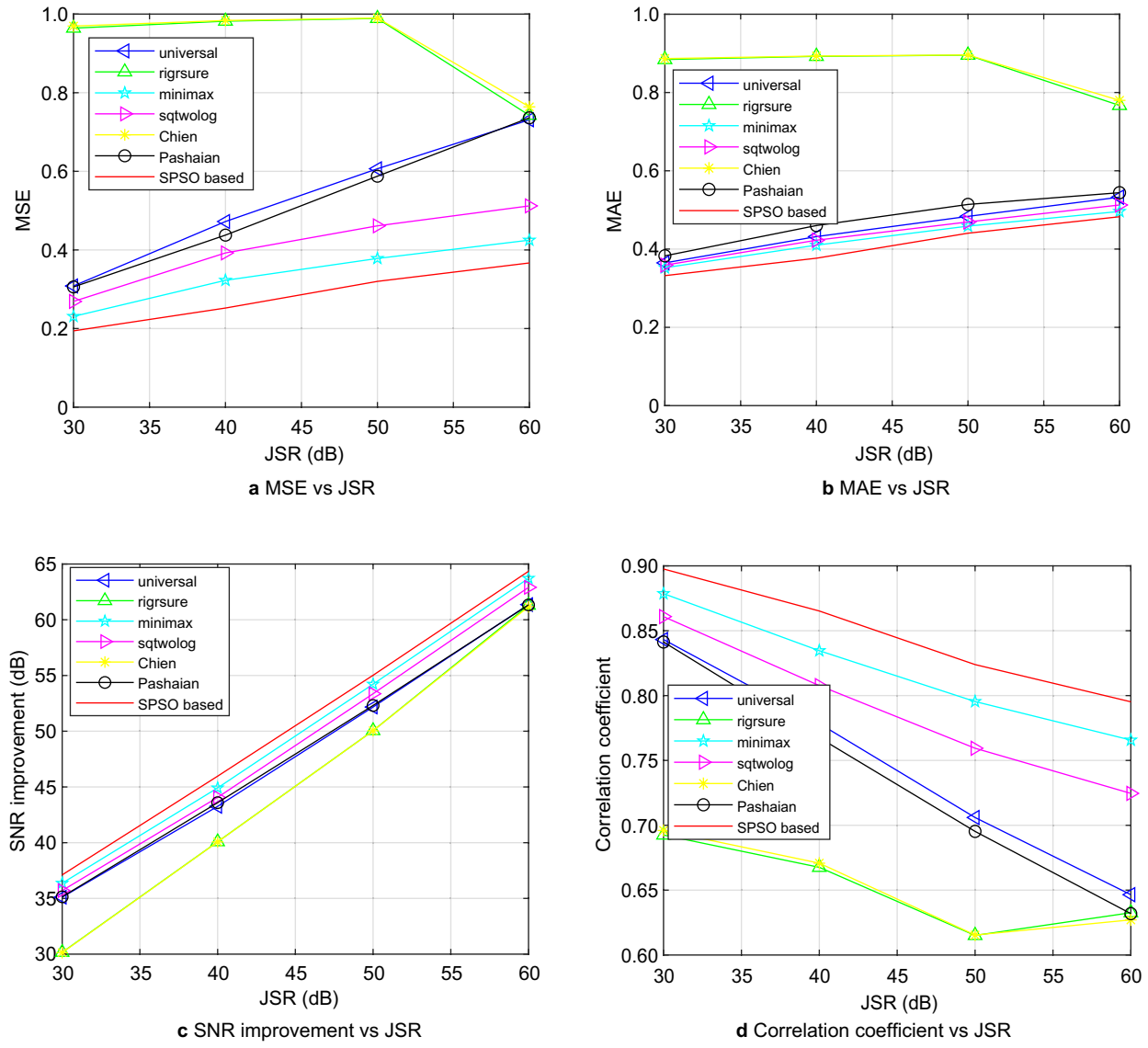

Fig. 9 Comparison of various thresholding rules under CCWI-2

30%, 16% under CCWI-2 in terms of CC over universal, rigrsure, minimax, sqtwolog, Chein and Pashaian methods are noticed. In terms of SNR improvement, a gain of 3.1 dB, 4.8 dB, 0.6 dB, 1.7 dB, 4.9 dB, 3.6 dB under CCWI-1 and 2.6 dB, 5.2 dB, 0.8 dB, 1.6 dB, 5.3 dB, 2.5 dB under CCWI-2 over the respective threshold rule methods are observed.

Selection of thresholding function

The Softsign thresholding function constructed in this paper was compared with the well-known non-parametric thresholding functions such as soft (Chien, 2018; Mosavi et al., 2015; Pashaian et al., 2016), hard (Mosavi et al., 2015; Pashaian et al., 2016), and parametric thresholding functions such as trimmed (Sumithra & Thanushkodi, 2009), Sigmoid (Yi et al., 2012) and hyperbolic (He et al., 2015) to validate the reliability of the proposed function. For all the previous thresholding functions, the threshold was obtained using the minimax threshold rule as it displays better performance than the other conventional thresholding rules as depicted in Fig. 6, 7, 8, 9. However, for the parametric SSTF, the optimal threshold and shape tuning parameter were obtained by the SPSO. Figures 10 and 11 show the comparative analysis of all the thresholding functions in terms of MSE and MAE. While Table 4 and Table 5 summarize the results obtained in

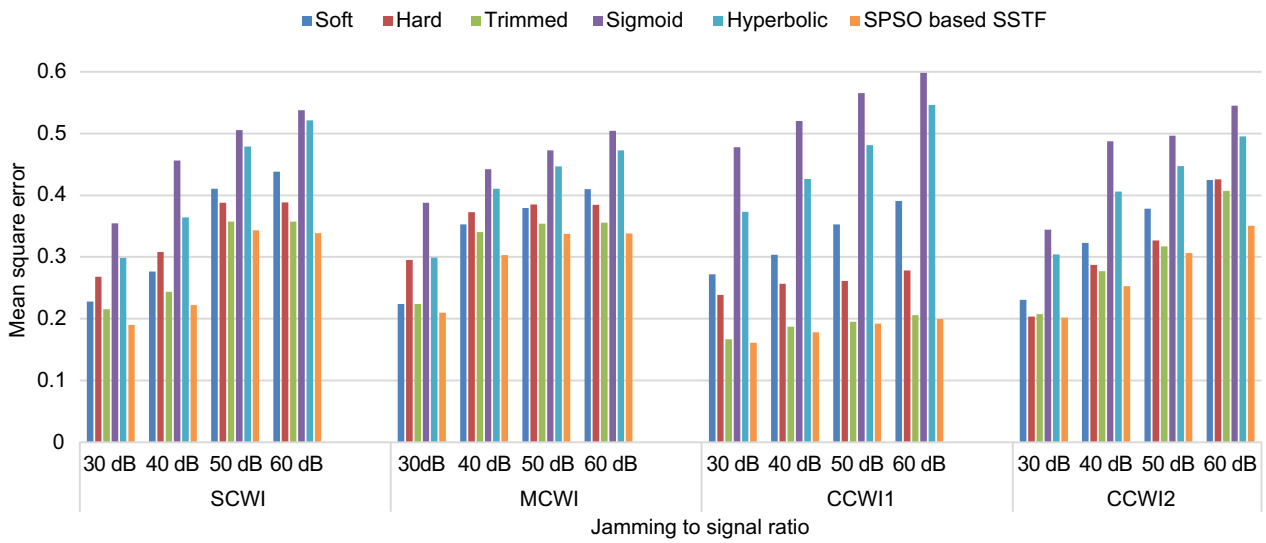

Fig. 10 MSE vs JSR comparison for various thresholding functions

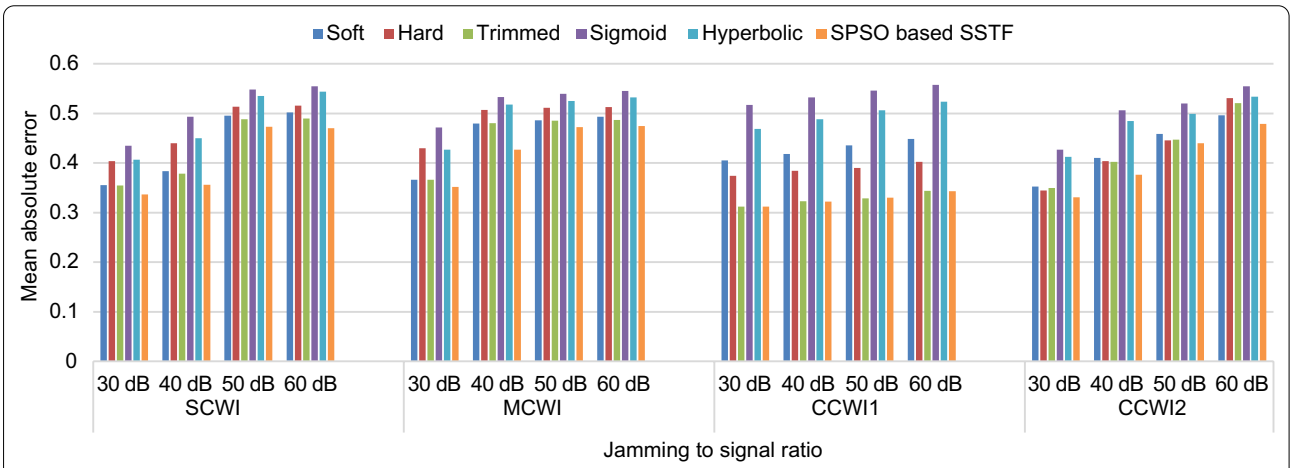

Fig. 11 MAE vs JSR comparison for various thresholding functions

terms of SNR improvement and CC. It can be seen from the results that the MSE and MAE values obtained by the SPSO-based SSTF are smaller, while the SNR improvement and CC values obtained are greater when compared with the other thresholding functions. This demonstrates that the proposed SSTF works well to modify the wavelet coefficients in a way that reduces noise and SCW, MCW, CCW-1, and CCW-2 jammers. That is, the optimization-based parametric wavelet packet thresholding works better than the wavelet packet thresholding approaches by Chien (2018); Mosavi et al. (2015); and Pashaian et al. (2016) under all jamming scenarios, as it induces the flexibility to process various signals.

The proposed SSTF shows an average improvement of 23% over soft, 19% over hard, 6% over trimmed, 46% over sigmoid, and 39% over hyperbolic thresholding functions in terms of MSE. Similarly, an average improvement of 10%, 12%, 4%, 24%, and 20% in terms of MAE is observed. Significant improvement is also observed in terms of SNR_{imp} and CC.

Selection of optimization algorithm

Six optimization algorithms were taken to validate the performance of the proposed Improved PSO algorithm. They are Firefly Algorithm (FA) (Jones & Boizanté, 2011), Differential Evolution (DE) (Jones & Boizanté, 2011), hybrid PSO and Gravitational Search algorithm

Table 4 SNR_{imp} vs JSR comparison for various thresholding functions

Jamming type	JSR (dB)	Soft Thresholding	Hard Thresholding	Trimmed Thresholding	Sigmoid Thresholding	Hyperbolic Thresholding	SPSO based SSTF
SCWI	30	36.42	35.72	36.66	34.50	35.25	**37.16**
	40	45.58	45.11	46.13	43.41	44.39	**46.50**
	50	53.87	54.12	54.47	52.96	53.20	**54.73**
	60	63.58	64.10	64.47	62.69	62.83	**64.67**
MCWI	30	36.50	35.30	36.50	34.11	35.24	**36.80**
	40	44.52	44.28	44.68	43.54	43.87	**45.15**
	50	54.21	54.14	54.51	53.25	53.50	**54.76**
	60	63.87	64.15	64.49	62.97	63.25	**64.66**
CCWI-1	30	35.67	36.24	37.80	33.22	34.30	**37.84**
	40	45.19	45.92	47.30	42.86	43.72	**47.34**
	50	54.54	55.85	57.11	52.49	53.19	**57.17**
	60	64.10	65.57	66.88	62.25	62.64	**66.91**
CCWI-2	30	36.37	36.91	36.83	34.63	35.17	**37.18**
	40	44.91	45.42	45.58	43.12	43.91	**46.10**
	50	54.22	54.86	54.99	53.04	53.49	**55.15**
	60	63.72	63.71	63.90	62.64	63.05	**64.52**

Table 5 CC vs JSR comparison for various thresholding functions

Jamming type	JSR (dB)	Soft thresholding	Hard thresholding	Trimmed thresholding	Sigmoid thresholding	Hyperbolic thresholding	SPSO based SSTF
SCWI	30	0.880	0.856	0.886	0.811	0.841	**0.901**
	40	0.855	0.832	0.870	0.760	0.809	**0.882**
	50	0.774	0.783	0.802	0.719	0.734	**0.812**
	60	0.759	0.782	0.802	0.703	0.714	**0.810**
MCWI	30	0.882	0.840	0.882	0.793	0.841	**0.892**
	40	0.805	0.792	0.812	0.752	0.770	**0.840**
	50	0.790	0.784	0.804	0.736	0.750	**0.813**
	60	0.774	0.785	0.803	0.720	0.737	**0.812**
CCWI-1	30	0.854	0.875	0.914	0.740	0.799	**0.916**
	40	0.838	0.864	0.904	0.720	0.774	**0.905**
	50	0.813	0.861	0.899	0.699	0.749	**0.902**
	60	0.795	0.852	0.893	0.686	0.723	**0.894**
CCWI-2	30	0.879	0.893	0.890	0.818	0.838	**0.898**
	40	0.835	0.852	0.854	0.750	0.776	**0.867**
	50	0.795	0.823	0.827	0.730	0.756	**0.836**
	60	0.766	0.775	0.780	0.697	0.724	**0.789**

(PSO-GSA) (Mirjalili & Hashim, 2010), SPSO (Bansal et al., 2011), Random PSO (RPSO) (Bansal et al., 2011) in which a random inertia weight is considered, and Linear decreasing inertia weight PSO (LPSO) (Bansal et al., 2011). The thresholding function for all the comparisons was taken as SSTF, and the simulation parameters were taken as that of IPSO, as presented in Table 2. The comparative analysis of IPSO with the well-known optimization algorithms and variants of PSO is summarized in Tables 6, 7, 8, 9. The optimal values obtained have been bolded. In terms of MSE, the IPSO algorithm shows an average improvement of 2.7% over FA, 2.2% over DE, 2.4% over PSO-GSA, 1.9% over SPSO, 2.7% over RPSO, and 2.6% over LPSO. In terms of MAE, it shows 1.9%, 1.6%, 1.6%, 0.5%, 1.5%, and 1.7% average improvement over the respective optimization algorithms. The

Table 6 MSE vs JSR comparison for PWPT approach based on various optimization algorithms

Jamming type	JSR(dB)	FA	DE	PSO-GSA	SPSO	RPSO	LPSO	IPSO
SCWI	30	0.2012	0.1940	0.1929	0.1903	0.1942	0.1950	**0.1896**
	40	0.2227	0.2247	0.2229	0.2225	0.2190	0.2221	**0.2185**
	50	0.3415	0.3419	0.3386	0.3430	0.3369	0.3391	**0.3365**
	60	0.3462	0.3373	0.3405	0.3388	0.3441	0.3388	**0.3355**
MCWI	30	0.2051	0.2069	0.2055	0.2096	0.2091	0.2086	**0.2030**
	40	0.3041	0.3015	0.3074	0.3032	0.3073	0.3070	**0.2960**
	50	0.3394	0.3367	0.3356	0.3375	0.3390	0.3358	**0.3317**
	60	0.3381	0.3426	0.3431	0.3379	0.3421	0.3419	**0.3370**
CCWI1	30	0.1602	0.1619	0.1636	0.1614	0.1610	0.1605	**0.1598**
	40	0.1770	0.1756	0.1748	0.1782	0.1808	0.1778	**0.1744**
	50	0.1917	0.1942	0.1930	0.1925	0.1902	0.1932	**0.1885**
	60	0.2008	0.2050	0.2029	0.1999	0.2054	0.2036	**0.1993**
CCWI2	30	0.2029	0.1981	0.2003	0.2018	0.1988	0.2027	**0.1924**
	40	0.2466	0.2415	0.2419	0.2526	0.2510	0.2474	**0.2369**
	50	0.3058	0.3057	0.3091	0.3062	0.3061	0.3078	**0.3044**
	60	0.3897	0.3798	0.3843	0.3508	0.3864	0.3839	**0.3465**

Table 7 MAE vs JSR comparison for PWPT approach based on various optimization algorithms

Jamming type	JSR(dB)	FA	DE	PSO-GSA	SPSO	RPSO	LPSO	IPSO
SCWI	30	0.3395	0.3397	0.3344	0.3366	0.3399	0.3384	**0.3342**
	40	0.3607	0.3604	0.3619	0.3564	0.3563	0.3580	**0.3545**
	50	0.4746	0.4746	0.4718	0.4729	0.4751	0.4747	**0.4694**
	60	0.4742	0.4699	0.4732	0.4704	0.4774	0.4790	**0.4680**
MCWI	30	0.3542	0.3550	0.3530	0.3518	0.3488	0.3499	**0.3486**
	40	0.4322	0.4313	0.4297	0.4268	0.4303	0.4317	**0.4236**
	50	0.4710	0.4714	0.4719	0.4725	0.4737	0.4702	**0.4696**
	60	0.4760	0.4747	0.4744	0.4747	0.4745	0.4758	**0.4716**
CCWI1	30	0.3163	0.3154	0.3142	0.3118	0.3148	0.3159	**0.3100**
	40	0.3269	0.3222	0.3275	0.3221	0.3259	0.3268	**0.3212**
	50	0.3400	0.3392	0.3389	**0.3299**	0.3405	0.3414	0.3307
	60	0.3487	0.3466	0.3499	0.3432	0.3477	0.3472	**0.3424**
CCWI2	30	0.3438	0.3407	0.3435	0.3305	0.3410	0.3455	**0.3304**
	40	0.3790	0.3750	0.3773	0.3763	**0.3718**	0.3734	0.3719
	50	0.4406	0.4414	0.4383	0.4397	0.4399	0.4372	**0.4370**
	60	0.5000	0.5024	0.5027	0.4784	0.5001	0.5037	**0.4779**

summarized results show that the proposed IPSO-based PWPT outperforms the other optimization-based PWPT algorithms under all jamming environments in terms of all the performance metrics.

Conclusions

CWI is the most indigenous threat to the GNSS system. In this paper, a novel parametric wavelet packet thresholding based on IPSO is proposed to mitigate CWI in IRNSS receivers. A simple parametric wavelet thresholding function based on the Softsign function is constructed, and its properties are also proven mathematically. Also, a new non-linear decreasing inertia weight modifying strategy is employed to overcome the local optimum problem of conventional PSO. Then, the improved PSO is used to determine the optimal threshold and shape tuning parameter of SSTF. The results indicate that the optimization-based threshold estimation overcomes the thresholding drifting issue encountered with the universal threshold proposed in the Mosavi method. Besides, the newly designed parameter adaptive

Table 8 SNR improvement vs JSR comparison for PWPT approach based on various optimization algorithms

Jamming type	JSR(dB)	FA	DE	PSO-GSA	SPSO	RPSO	LPSO	IPSO
SCWI	30	37.082	37.265	**37.267**	37.159	37.172	37.155	37.203
	40	46.521	46.479	46.533	46.495	46.548	46.481	**46.611**
	50	54.617	54.700	54.658	54.732	54.650	54.706	**54.745**
	60	64.660	64.731	54.696	64.669	64.704	64.647	**64.748**
MCWI	30	36.746	36.877	36.885	36.799	36.851	36.820	**36.914**
	40	45.167	45.157	45.069	45.147	45.157	45.207	**45.219**
	50	54.691	54.704	54.726	54.759	54.708	54.716	**54.786**
	60	64.600	64.642	64.682	64.659	64.701	64.670	**64.736**
CCWI1	30	37.877	37.902	37.910	37.843	37.960	37.957	**37.969**
	40	47.486	47.504	47.477	47.340	47.529	47.537	**47.637**
	50	57.075	57.155	57.187	57.171	57.151	57.165	**57.230**
	60	66.931	66.921	66.912	66.905	66.954	66.914	**67.037**
CCWI2	30	36.980	36.923	36.898	37.178	36.986	36.971	**37.222**
	40	46.136	46.078	46.124	46.099	46.071	46.003	**46.155**
	50	55.112	55.126	55.161	55.154	55.057	55.158	**55.226**
	60	64.121	64.178	64.173	64.516	64.244	64.159	**64.572**

Table 9 CC vs JSR comparison for PWPT approach based on various optimization algorithms

Jamming type	JSR(dB)	FA	DE	PSO-GSA	SPSO	RPSO	LPSO	IPSO
SCWI	30	0.8932	0.9001	0.8969	0.9009	0.8989	0.8986	**0.9017**
	40	0.8813	0.8814	0.8814	0.8823	0.8801	0.8793	**0.8855**
	50	0.8136	0.8126	0.8120	0.8118	0.8124	0.8144	**0.8146**
	60	0.8114	0.8112	0.8123	0.8103	0.8110	0.8106	**0.8131**
MCWI	30	0.8921	0.8905	0.8874	0.8919	0.8901	0.8925	**0.8925**
	40	0.8353	0.8321	0.8332	0.8340	0.8315	0.8338	**0.8402**
	50	0.8137	0.8138	0.8139	0.8131	0.8150	0.8140	**0.8153**
	60	0.8111	0.8102	0.8107	0.8121	0.8117	0.8102	**0.8131**
CCWI1	30	0.9154	0.9158	0.9150	0.9162	0.9147	0.9162	**0.9170**
	40	0.9036	0.9060	0.9070	0.9054	0.9070	0.9058	**0.9074**
	50	0.8986	0.8982	0.8991	0.9016	0.8973	0.8980	**0.9032**
	60	0.8931	0.8917	0.8903	0.8939	0.8912	0.8931	**0.8946**
CCWI2	30	0.8939	0.8965	0.8942	0.8978	0.8942	0.8946	**0.8990**
	40	0.8672	0.8670	0.8660	0.8666	0.8675	0.8660	**0.8689**
	50	0.8302	0.8318	0.8320	0.8319	0.8305	0.8329	**0.8360**
	60	0.7873	0.7892	0.7855	0.8053	0.7863	0.7855	**0.8061**

thresholding function, i.e., SSTF, overcomes the limitations of hard and soft thresholding functions. Therefore, a smooth signal can be reconstructed without discontinuity at the threshold value and reduced deviation between the estimated and original wavelet coefficients. Also, SSTF outperforms the well-known parametric thresholding functions like trimmed, sigmoid, and hyperbolic. In addition, the previous WPT-based jamming mitigation techniques require 7–10 decomposition levels to have acceptable interference mitigation, whereas the proposed method seems to work well at a lower decomposition level of 4 under all the jamming scenarios. The results show that the proposed IPSO-based PWPT approach has better capability to combat both stationary and non-stationary jammers than the conventional WPT.

Abbreviations

ADC: Analog to digital converter; AWGN: Additive white Gaussian noise; BDS: BeiDou Navigation Satellite System; CA: Code acquisition; CC: Correlation coefficient; CPU: Central processing unit; CWI: Continuous wave interference; CCWI: Chirp CWI; CWT: Continuous wavelet transform; DE: Differential evolution; DME: Distance measuring equipment; DWT: Discrete wavelet transform; FA: Firefly algorithm; GLONASS: Global navigation satellite system (Russian:Globalnaya Navigatsionnaya Sputnikovaya Sistema); GNSS:

Global navigation satellite systems; GPS: Global Positioning System; GSA: Gravitational search algorithm; HPF: High pass filter; IF: Intermediate frequency; IPSO: Improved particle swarm optimization; IRNSS: Indian Regional Navigational Satellite System; ISRO: Indian Space Research Organization; ISM: Industrial scientific medical; JSR: Jamming to signal power ratio; JTIDS: Joint Tactical Information Distribution System; LPF: Low pass filter; MAE: Mean absolute error; MCWI: Multi-tone CWI; MIDS: Multifunctional Information Distribution System; MSE: Mean square error; MST: Matched signal transform; PPD: Personal privacy devices; PRN: Pseudo-random noise; PSO: Particle swarm optimization; QZSS: Quasi-Zenith Satellite System; RAM: Random access memory; RPSO: Random PSO; SCWI: Single-tone CWI; SPS: Standard Positioning Service; SPSO: Standard PSO; SSIW: Softsign inertia weight; SSTF: Softsign thresholding function; STFT: Short-time Fourier transform; TACAN: Tactical air navigation; TD: Transform domain; TF: Time–frequency; WPT: Wavelet packet transform; WT: Wavelet transform; WVD: Wigner ville distribution; Wi-Fi: Wireless fidelity.

Acknowledgements
Not applicable.

Author contributions
JSLK proposed the general idea of this contribution and completed the algorithm design, evaluation, and was a major contributor in writing the manuscript. MR is the supervisor who modified this paper. Both the authors read and approved the final manuscript.

Funding
Not applicable.

Availability of data and materials
The IRNSS and jamming signal data were generated by simulation. However, if required, the datasets used and/or analyzed during the current study are available from the corresponding author upon reasonable request.

Declarations

Competing interests
The authors declare that they have no competing interests.

Received: 20 February 2022 Accepted: 14 August 2022
Published online: 10 October 2022

References

Abedi, M., Rezaei, M. J., & Mosavi, M. R. (2018). Accurate interference mitigation in Global Positioning System receivers based on double-step Short-Time Fourier Transform. *Circuits, Systems, and Signal Processing, 37*(6), 2450–2470. https://doi.org/10.1007/s00034-017-0670-y

Anyaegbu, E., Brodin, G., Cooper, J., Aguado, E., & Boussakta, S. (2008). An integrated pulsed interference mitigation for GNSS receivers. *The Journal of Navigation, 61*(2), 239–255. https://doi.org/10.1017/S0373463307004572

Bansal, J. C., Singh, P. K., Saraswat, M., Verma, A., Jadon, S. S., & Abraham, A. (2011). Inertia weight strategies in Particle Swarm Optimization. In: *Proceedings of the Third World Congress on Nature and Biologically Inspired Computing,* Salamanca, Spain, 633–640. https://doi.org/10.1109/NaBIC.2011.6089659

Borio, D. (2021). GNSS interference mitigation: A measurement and position domain assessment. *Navigation, 68*(1), 93–114. https://doi.org/10.1002/navi.391

Borio, D., Camoriano, L., & Lo Presti, L. (2008). Two-pole and multi-pole notch filters: A computationally effective solution for GNSS interference detection and mitigation. *IEEE Systems Journal, 2*(1), 38–47. https://doi.org/10.1109/ITST.2007.4295837

Capozza, P. T., Holland, B. J., Hopkinson, T. M., & Landrau, R. L. (2000). A single-chip narrow-band frequency-domain excisor for a Global Positioning System (GPS) receiver. *IEEE Journal of Solid-State Circuits, 35*(3), 401–411. https://doi.org/10.1109/4.826823

Chatterjee, A., & Siarry, P. (2006). Nonlinear inertia weight variation for dynamic adaptation in particle swarm optimization. *Computers and Operations Research, 33*(3), 859–871. https://doi.org/10.1016/j.cor.2004.08.012

Chien, Y. R. (2018). Wavelet packet transform-based anti-jamming scheme with new threshold selection algorithm for GPS receivers. *Journal of the Chinese Institute of Engineers, 41*(3), 181–185. https://doi.org/10.1080/02533839.2018.1454857

Chien, Y. R., Chen, P. Y., & Fang, S. H. (2017). Novel anti-jamming algorithm for GNSS receivers using wavelet-packet-transform-based adaptive predictors. *IEICE Transactions on Fundamentals of Electronics, Communications and Computer Sciences, E100*(A(2)), 602–610. https://doi.org/10.1587/transfun.E100.A.602

Dey, A., Singh, P., & Sharma, N. (2019) Performance evaluation of tracking loop under RF interference using NavIC software-receiver. In: *Proceedings of the 2019 IEEE Asia-Pacific Microwave Conference (APMC)*, Singapore, 1050–1052. https://doi.org/10.1109/APMC46564.2019.9038472

Dey, A., Iyer, K., & Sharma, N. (2021) S-band interference detection and mitigation using a vector tracking-based NavIC software receiver. In: *Proceedings of the 34th International Technical Meeting of the Satellite Division of the Institute of Navigation*, ION GNSS+ 2021. St. Louis, Missouri, 3464–3476

Eberhart, R. C., & Shi, Y. (2001). Tracking and optimizing dynamic systems with particle swarms. In: *Proceedings of the 2001 Congress on Evolutionary Computation (IEEE Cat. No.01TH8546)*. Seoul, Korea (South), 94–100. https://doi.org/10.1109/CEC.2001.934376

El-Dahshan, E.-S.A. (2011). Genetic algorithm and wavelet hybrid scheme for ECG signal denoising. *Telecommunication Systems, 46*(3), 209–215. https://doi.org/10.1007/s11235-010-9286-2

Fadaei, N. (2016). Detection, Characterization and Mitigation of GNSS Jamming Interference Using Pre-Correlation Methods (Unpublished master's thesis). University of Calgary, Calgary, AB. https://prism.ucalgary.ca/bitstream/handle/11023/2894/ucalgary_2016_fadaei_nahal.pdf?sequence=3&isAllowed=y

Gao, G. X., Sgammini, M., Lu, M., & Kubo, N. (2016). Protecting GNSS receivers from jamming and interference. In: *Proceedings of the IEEE, 104*(6), 1327–1338. https://doi.org/10.1109/JPROC.2016.2525938

He, C., Xing, J., Li, J., Yang, Q., & Wang, R. (2015). A new wavelet thresholding function based on Hyperbolic tangent function. *Mathematical Problems in Engineering, 2015*, 1–10. https://doi.org/10.1155/2015/528656

Jagiwala, D. D., & Shah, S. N. (2021). Wavelet-based interference perception and reduction approach for NB and CW RFI on NavIC S-band Signals. In: *2021 IEEE International Conference on Electronics, Computing and Communication Technologies (CONECCT)*. Bangalore, India, 1–6. https://doi.org/10.1109/CONECCT52877.2021.9622729

Jagiwala, D. D., & Shah, S. N. (2019). Perception and reduction of Wi-Fi interference on NavIC signals. *IET Radar, Sonar and Navigation, 13*(3), 352–356. https://doi.org/10.1049/iet-rsn.2018.5291

Jones, K. O., & Boizanté, G. (2011). Comparison of firefly algorithm optimisation, particle swarm optimisation and differential evolution. In: *Proceedings of the 12th International Conference on Computer Systems and Technologies-CompSysTech'2011*, 578, 191–197. https://doi.org/10.1145/2023607.2023640

Kaiser, G. (1994). *A Friendly guide to wavelets* (1st ed.). Birkhäuser Boston, MA. https://doi.org/10.1007/978-0-8176-8111-1.

Kennedy, J., & Eberhart, R. (1995). Particle Swarm Optimisation. In: *Proceedings of ICNN'95 - International Conference on Neural Networks. Perth, WA, Australia*, 1942–1948. https://doi.org/10.1007/978-3-030-61111-8_2

Kumar, C. H. J., & Veerakumari, M. (2012). Load forecasting of Andhra Pradesh grid using PSO, DE algorithms. *International Journal of Advanced Research in Computer Engineering and Technology, 1*(9), 179–184.

Li, M., Dempster, A. G., Balaei, A. T., Rizos, C., & Wang, F. (2011). Switchable beam steering/null steering algorithm for CW interference mitigation in GPS C/A code receivers. *IEEE Transactions on Aerospace and Electronic Systems, 47*(3), 1564–1579. https://doi.org/10.1109/TAES.2011.5937250

Lineswala, P. L., Jagiwala, D. D., & Shah, S. N. (2019). Hypothesis test-based detection of Wi-Fi interference on NavIC/IRNSS S-band signal. *Journal of Navigation, 72*(4), 931–947. https://doi.org/10.1017/S037346331900002X

Lineswala, P. L., & Shah, S. N. (2019). Performance analysis of different interference detection techniques for navigation with Indian constellation. *IET Radar, Sonar and Navigation, 13*(8), 1207–1213. https://doi.org/10.1049/iet-rsn.2019.0091

Lv, Q., & Qin, H. (2019). An improved method based on Time-Frequency distribution to detect time-varying interference for GNSS receivers with single antenna. *IEEE Access, 7*, 38608–38617. https://doi.org/10.1109/ACCESS.2019.2906262

Mao, W. L. (2008). Novel SREKF-based recurrent neural predictor for narrowband/FM interference rejection in GPS. *AEU International Journal of Electronics and Communications, 62*(3), 216–222. https://doi.org/10.1016/j.aeue.2007.04.002

Mirjalili, S., & Hashim, S. Z. M. (2010). A new hybrid PSOGSA algorithm for function optimization. In: *2010 International Conference on Computer and Information Application*.Tianjin, China, 374–377. https://doi.org/10.1109/ICCIA.2010.6141614

Morales-ferre, R., Richter, P., Falletti, E., De la Fuente, A., & Lohan, E. S. (2019). A survey on coping with intentional interference in satellite navigation for manned and unmanned aircraft. *IEEE Communications Surveys and Tutorials, 22*(1), 249–291. https://doi.org/10.1109/COMST.2019.2949178

Mosavi, M. R., Pashaian, M., Rezaei, M. J., & Mohammadi, K. (2015). Jamming mitigation in global positioning system receivers using wavelet packet coefficients thresholding. *IET Signal Processing, 9*(5), 457–464. https://doi.org/10.1049/iet-spr.2014.0280

Mosavi, M. R., Rezaei, M. J., Pashaian, M., & Moghaddasi, M. S. (2017). A fast and accurate anti-jamming system based on wavelet packet transform for GPS receivers. *GPS Solutions, 21*(2), 415–426. https://doi.org/10.1007/s10291-016-0535-z

Musumeci, L., & Dovis, F. (2013). Performance assessment of wavelet based techniques in mitigating narrow-band interference. In: *2013 International Conference on Localization and GNSS*, ICL-GNSS. Turin, Italy, 1–6. https://doi.org/10.1109/ICL-GNSS.2013.6577264

Musumeci, L., & Dovis, F. (2014). Use of the wavelet transform for interference detection and mitigation in global navigation satellite systems. *International Journal of Navigation and Observation, 2014*, 1–14. https://doi.org/10.1155/2014/262186

Nisha, S. S., & Mohideen, S. K. (2016). Wavelet coefficients thresholding techniques for denoising MRI images. *Indian Journal of Science and Technology*, 9(28), 1–8. https://doi.org/10.17485/ijst/2016/v9i28/93872

Ouyang, X., & Amin, M. G. (2001). Short-time Fourier transform receiver for nonstationary interference excision in direct sequence spread spectrum communications. *IEEE Transactions on Signal Processing, 49*(4), 851–863. https://doi.org/10.1109/78.912929

Pashaian, M., Mosavi, M. R., Moghaddasi, M. S., & Rezaei, M. J. (2016). A novel interference rejection method for GPS receivers. *Iranian Journal of Electrical and Electronic Engineering, 12*(1), 9–20. https://doi.org/10.22068/IJEEE.12.1.9

Pena, A. G., Macabiau, C., Julien, O., Mabilleau, M., & Durel, P. (2020). Impact of DME/TACAN on GNSS L5/E5a receiver. In: *Proceedings of the 2020 International Technical Meeting ION ITM,*. San Diego, California, 207–221.

Satirapod, C., & Rizos, C. (2005). Multipath mitigation by wavelet analysis for GPS base station applications. *Survey Review, 38*(295), 2–10. https://doi.org/10.1179/003962605791521699

Satish, R., & Kumar, P. R. (2020). Efficient method for segmentation of noisy and non-circular iris images using improved particle swarm optimisation-based MRFCM. *IET Biometrics, 9*(2), 78–90. https://doi.org/10.1049/iet-bmt.2019.0026

Sharifi-tehrani, O., Farzan Sabahi, M., & Raees Danaee, M. (2020). Low-complexity framework for GNSS jamming and spoofing detection on moving platforms. *IET Radar, Sonar and Navigation, 14*(12), 2027–2038. https://doi.org/10.1049/iet-rsn.2020.0285

Sharma, I., Kuldeep, B., Kumar, A., & Singh, V. K. (2016). Performance of swarm based optimization techniques for designing digital FIR filter: A comparative study. *Engineering Science and Technology, an International Journal, 19*(3), 1564–1572. https://doi.org/10.1016/j.jestch.2016.05.013

Shen, H., & Papandreou-suppappola, A. (2005). Wideband time-varying interference suppression using Matched Signal Transforms. *IEEE Transactions on Signal Processing, 53*(7), 2607–2612. https://doi.org/10.1109/TSP.2005.849218

Shi, Y., & Eberhart, R. (1998). A modified particle swarm optimizer. In: *1998 IEEE International Conference on Evolutionary Computation Proceedings*. IEEE World Congress on Computational Intelligence (Cat. No.98TH8360), Anchorage, AK, USA, 69–73. https://doi.org/10.1109/ICEC.1998.699146

Shi, Y., & Eberhart, R. C. (1999). Empirical study of particle swarm optimization. In: *Proceedings of the 1999 Congress on Evolutionary Computation-CEC99 (Cat. No. 99TH8406)*. Washington, DC, USA, 1945-1950. https://doi.org/10.1109/CEC.1999.785511

Silva Lorraine, K. J., & Ramarakula, M. (2021a). A comprehensive survey on GNSS interferences and the application of neural networks for anti- jamming. *IETE Journal of Research*. https://doi.org/10.1080/03772063.2021.1953407

Silva Lorraine, K. J., & Ramarakula, M. (2021b). An efficient interference mitigation approach for NavIC receivers using improved variational mode decomposition and wavelet packet decomposition. *Transactions on Emerging Telecommunications Technologies, 32*(4), 1–24. https://doi.org/10.1002/ett.4242

Silva Lorraine, K. J., & Ramarakula, M. (2021c). Hybrid anti-jamming algorithm for Indian Regional Navigation Satellite System receivers using variational mode decomposition and wavelet packet transform. *International Journal of Communication Systems, 34*(7), 1–16. https://doi.org/10.1002/dac.4734

Song, W. E. I., & Hua, Z. (2020). Multi-exemplar particle swarm optimization. *IEEE Access, 8*, 176363–176374. https://doi.org/10.1109/ACCESS.2020.3026620

Sumithra, A. M. G., & Thanushkodi, B. K. (2009). Performance evaluation of different thresholding methods in time adaptive wavelet based speech enhancement. *IACSIT International Journal of Engineering and Technology, 1*(5), 439–447.

Varshney, N., & Jain, R. . (2013). An adaptive notch filter for narrow band interference removal. In: *2013 National Conference on Communications (NCC)*. New Delhi, India, 1–5. https://doi.org/10.1109/NCC.2013.6487917

Wang, P., Wang, Y., Cetin, E., Dempster, A. G., & Wu, S. (2019). Time-Frequency jammer mitigation based on Kalman Filter for GNSS receivers. *IEEE Transactions on Aerospace and Electronic Systems, 55*(3), 1561–1567. https://doi.org/10.1109/TAES.2018.2869507

Yi, T.-H., Li, H.-N., & Zhao, X.-Y. (2012). Noise smoothing for structural vibration test signals using an improved wavelet thresholding technique. *Sensors, 12*(8), 11205–11220. https://doi.org/10.3390/s120811205

Zhang, J., Cui, X., Xu, H., & Lu, M. (2019). A two-stage interference suppression scheme based on antenna array for GNSS jamming and spoofing. *Sensors (basel, Switzerland), 19*(18), 3870. https://doi.org/10.3390/s19183870

Zhang, J., Sheng, J., Lu, J., & Shen, L. (2021). UCPSO-a uniform initialized particle swarm optimization algorithm with cosine inertia weight. *Computational Intelligence and Neuroscience, 2021*, 1–18. https://doi.org/10.1155/2021/8819333

Zhang, X., Li, J., Xing, J., Wang, P., Yang, Q., & He, C. (2017). A Particle Swarm Optimization technique-based parametric wavelet thresholding function for signal denoising. *Circuits, Systems, and Signal Processing, 36*(1), 247–269. https://doi.org/10.1007/s00034-016-0303-x

Zhang, X., Li, J., Xing, J., Wang, P., Yang, Q., Wang, R., & He, C. (2014). Optimal sensor placement for latticed shell structure based on an improved particle swarm optimization algorithm. *Mathematical Problems in Engineering, 2014*, 1–12. https://doi.org/10.1155/2014/743904

Zhang, Y., & Wang, A. (2020). Research on the fault diagnosis method for rolling bearings based on improved VMD and automatic IMF acquisition. *Shock and Vibration, 2020*, 1–19. https://doi.org/10.1155/2020/6216903

Publisher's Note